Journal of the Physical Society of Japan
Vol. 70, No. 9, September, 2001, pp. 2559–2567

Absolute Total and Partial Cross Sections for Ionization of Free Lanthanide Atoms by Electron Impact

Shuichi Yagi and Tetsuo Nagata

Department of Physics, Meisei University, Tokyo 191-8506

(Received September 18, 2000)

Absolute values of the total-apparent, total-counting, and charge separated partial cross sections have been measured for electron impact ionization of free atoms of Ce, Nd, Sm, Gd, Dy, Er and Yb. The electron energies have ranged from the single ionization threshold to 900 eV. Absolute total cross sections were determined with a crossed electron-atom beam assembly combined with time-of-flight velocity and oscillating crystal sensor accumulation measurements of target atoms. The relative partial cross sections were obtained separately with a magnetic deflection mass selector, and they were normalized to the total cross sections. The absolute cross sections have been determined with accuracy 23–33% depending on the target atom. Some of the single ionization cross section curves show complicated resonance-like structure in the region of $4f$ ionization thresholds. The $4d$ ionization exhibits a peak of shape resonance feature in the Ce^{3+} and Nd^{3+} curves, but the peak becomes less prominent with the increase in the atomic number Z and disappears beyond the Eu atom; this may be attributed to the lowering of the centrifugal barrier potential for f electrons in higher Z elements. Evidences of shake-up and/or shake-off processes associated with $5p$ or $5s$ electrons are observed in the quadruple ionization.

KEYWORDS: cross section, electron impact, ionization, lanthanide

§1. Introduction

In one of our previous papers,[1] we reported an experimental study of the electron impact ionizations of Ba and Eu atoms. We have described there in detail our apparatus and procedure as well as the experimental results. In the present work, we have extended our measurement to the species Ce, Nd, Sm, Gd, Dy, Er and Yb which enabled us to the systematics of the electron impact ionization phenomena in lanthanide elements.

More than 70 years have passed since Jones[2] firstly measured the electron impact ionization of mercury atoms, and the measurement has been extended to cover various atoms by many authors. However, there remain yet 25 elements unexplored still now. Most of such the elements require high temperatures (> 1200 K) for vaporization. For lanthanides (^{57}La–^{71}Lu), 11 of the 15 elements are open for extensive studies. Concerning the cross-section measurement, we find only a report by Shimon *et al.*[3] They measured Sm, Eu, Tm, and Yb atoms in the energy range up to 200 eV. Measurements of lanthanides are therefore highly desirable for further understanding of the ionization phenomena in atoms and for providing the related fields with the cross section data. From the physical point of view, it is very interesting to examine the atomic-number dependence of the ionization phenomena in the lanthanide series.

In the electron impact ionization of atoms, two different total cross sections are defined.[4] One is the "total" cross section, which is defined as

$$\sigma_{\mathrm{T}} = \sum_q q\sigma_{q+}, \tag{1}$$

where σ_{q+} is the partial cross section for the formation of atomic ions with a charge state A^{q+}. The σ_{T} is often called "apparent" or "gross" cross section. The other is the "counting" cross section which is defined as

$$\sigma_{\mathrm{C}} = \sum_q \sigma_{q+}. \tag{2}$$

The present paper reports the results of σ_{T}, σ_{C} and σ_{q+} for the seven lanthanide atoms. The total cross sections σ_{T} have been measured with accuracy 23–33% depending on the target. One of the prominent features observed in this study is the resonance behavior of $4d$ ionization in the triple ionization curves of lighter lanthanide species (Ce, Nd) and its disappearance in heavier species.

§2. Experimental

2.1 General

The details of the apparatus and procedure have been described in a previous paper.[1] Briefly, the relative partial cross sections for single to quadruple ionization were measured with a crossed electron-atom beam ion source combined with a 60° sector mass analyzer. Intensity of an individual ionic species was measured with varying the electron energy in the range from its ionization threshold to 900 eV.

For the measurement of absolute total cross sections, a different crossed electron-atom beam assembly was used. Using the time of flight (TOF) technique combined with a pulsed electron gun, we determined the average velocity of target atoms. At the same time, using a quartz crystal sensor (CRTM-5000. ULVAC), we measured the accumulation rate of target atoms on the crystal surface of the sensor. From these data, we were able to estimate the target atom density. The results of the absolute measurements were used to calibrate the corresponding partial cross sections.

Table I. The operating conditions of the oven in the measurements on the lanthanide elements.

	Ce	Nd	Sm	Eu	Gd	Dy	Er	Yb
Intensity ratio[a)]	39.9	71.0	74.0	99.5	36.9	71.0	50.9	54.0
Phase[b)]	L	L	S	S	L	L	L or S	S
Crucible[c)]	Ta	C&Ta	SUS	SUS	C&Ta	C&Ta	Ta	SUS
Operat. temp. (K)	1700	1500	1100	1000	1700	1400	1400	800

a) The ratio of the atomic-beam intensity I_C at the collision center relative to that I_S at the atomic-beam detector (see §2.2).
b) Symbol S stands for solid, and L for liquid.
c) Material of the crucible. Symbol "C&Ta" means that the inside of carbon crucible is covered by a sheet tantalum.

In the present study, the temperature as high as 800–1700 K is required to vaporize the metal samples, and hence we used an efficient high-temperature oven of electron bombardment type. Material of the crucible was carbon, tantalum or stainless steel, depending on the metallic sample used.[5)] Sample of 2–3 g in the crucible lasted about two days. Table I summarizes, for each element, the approximate operating temperature of the oven, the material of crucible used, and the phase of metallic sample in the crucible at the operating temperature. The previous data on Eu atom[1)] is also included.

The main chamber in which the oven and other assemblies (the ion source in the partial measurement, or the ionization-region assembly and the atomic beam monitor in the absolute measurement) were contained was evacuated with a turbo molecular pump of 300 l/s. The background pressure in the chamber was lower than 1.5×10^{-4} Pa.

2.2 Determination of the absolute total cross sections

When an electron beam of current I_e passes through the target-atom region of density N, and generates ion current I_i, the apparent total cross section σ_T is given by

$$\sigma_T = \frac{I_i}{I_e \cdot L \cdot N}. \tag{3}$$

where L is the effective collision length. This relation is applicable if N is homogeneous in space in the interaction region and if single-collision condition is ensured there.[6)]

The absolute total "counting" cross section σ_C is given by

$$\sigma_C = \frac{I_i}{I_e \cdot N \cdot L \cdot \langle q \rangle_{av}} = \frac{\sigma_T}{\langle q \rangle_{av}}, \tag{4}$$

where $\langle q \rangle_{av}$ is the average ion charge calculated from the measured charge state distribution using the relation

$$\langle q \rangle_{av} = \sum_q q \cdot f_q \quad \left(f_q = \frac{\sigma_{q+}}{\sigma_C} \right), \tag{5}$$

where f_q is the fraction of ions with charge q. From eqs. (4) and (5), we are able to determine the partial cross sections σ_{q+}.

The target atom density N in eqs. (3) and (4) is given by

$$N = \frac{T \cdot \rho}{M \cdot \eta \cdot \langle v \rangle_{av}} \cdot \frac{I_C}{I_S}, \tag{6}$$

where T is the accumulation rate of target atoms on the crystal-sensor surface, ρ is the density of a given element in solid phase, I_S and I_C are the intensities of the atomic beam at the sensor surface and the collision center, respectively, η is the accumulation coefficient (sticking probability) of atoms on the sensor surface, and M is the mass of target atom. The coefficient η is taken to be unity.[1)]

The exit aperture (10 mm in diameter) of the oven used in the present experiment is lager than usual. For metallic elements which require high temperatures for vaporization, use of such a large aperture is inevitable to avoid blocking of the exit aperture by condensed atoms. This necessitated the measurement of the ratio I_C/I_S. The ratio was measured separately with a couple of surface ionization detectors for each element at the same operating condition of the oven as that in the cross-section measurement.

§3. Results

Figure 1 shows the absolute total (apparent σ_T and counting σ_C) cross sections and the absolute partial cross sections σ_{q+} obtained for the seven lanthanides (Ce, Nd, Sm, Gd, Dy, Er and Yb). Each data point of σ_T is an average of three to five determinations, and the error bar contains systematic errors only. Each partial curve is an average of three to five independent runs. The ionization thresholds of the subshell electrons from photoelectron spectroscopy data[13–16)] are indicated at the top of each figure. Table II summarizes the lowest ionization thresholds (that is, binding energies) of the individual subshell electrons and the appearance potentials of ions with charge q ($q = 1, 2, 3, 4$). From the viewpoint of applications and comparisons with theoretical calculations, the cross sections given numerically will sometimes be convenient. Values of the present total cross sections σ_T and σ_C are tabulated in Table III and Table IV, respectively.

Comparison of the present results with other data are possible only in the cases of Sm and Yb atoms. Figure 1 includes the partial cross sections σ_{q+} ($q = 1, 2, 3$) for these atoms reported by Shimon *et al.* We see that there are marked differences between their cross sections and the present ones both in the absolute magnitude and in the energy dependence. In particular, the cross section σ_+ for formation of Sm^+ ions amounts to about 2.3 times the present one. The structure in the 10–20 eV region of the present Sm^+ curve, as well as those in the other single ionization curves, was observed every times the

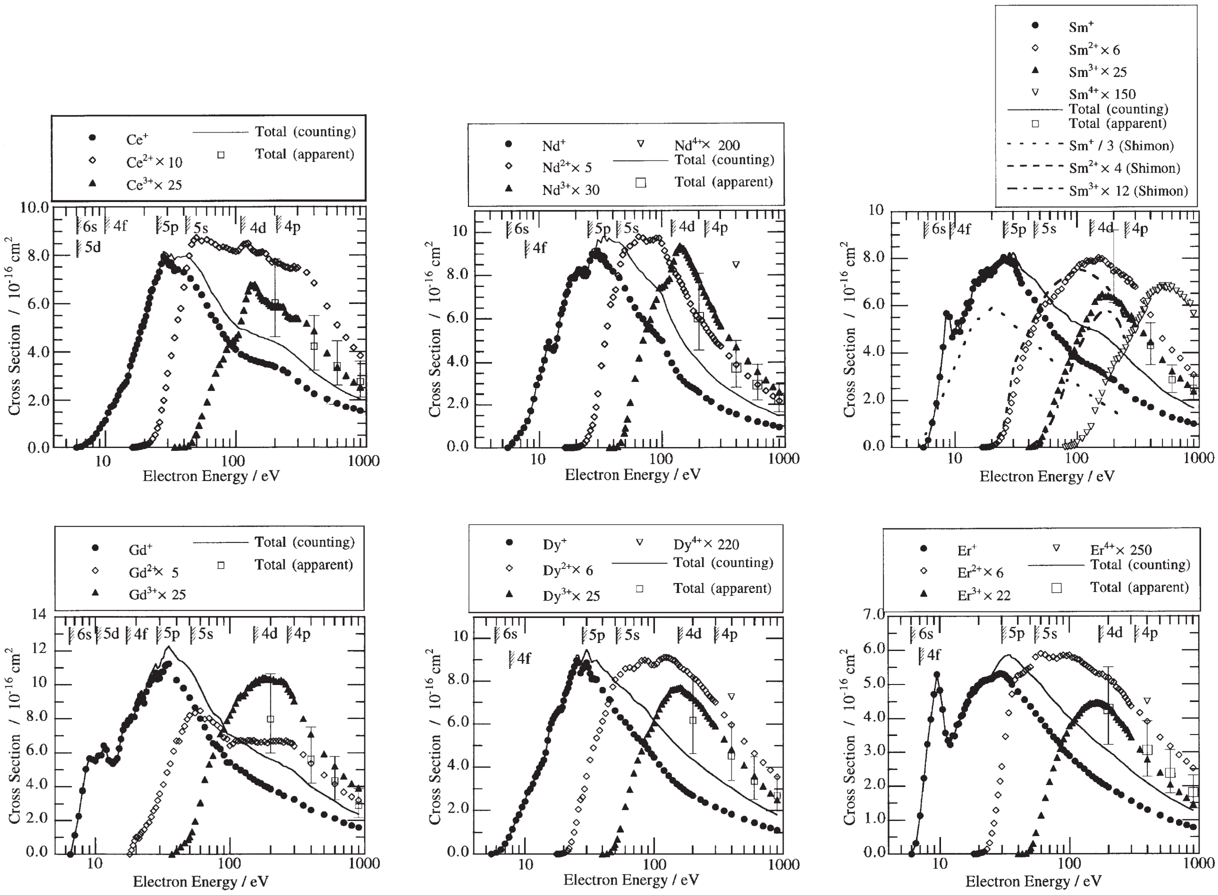

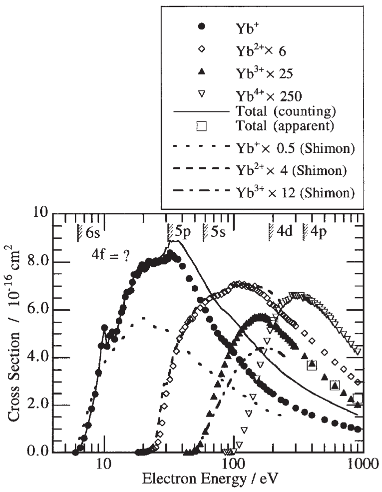

Fig. 1. The present absolute total (apparent σ_T and counting σ_C) and charge-separated partial cross sections σ_{n+} for electron impact ionization of Ce, Nd, Sm, Gd, Dy, Er and Yb atoms. In the cases of Sm and Yb, the experimental results obtained by Shimon *et al.* (ref. 3) are also included. The vertical lines at the top indicate the positions of the lowest ionization thresholds determined by photoelectron spectra (refs. 13–16). The error bars of the total (apparent) cross sections indicate systematic errors only.

measurement was done.

§4. Discussion

4.1 Accuracy of the present cross-section measurement

Table III includes the total systematic uncertainties estimated for the present measurements of σ_T. Each uncertainty is a quadrature sum which is calculated from uncertainties estimated for the individual quantities in eq. (3).

The total uncertainty estimated ranges from ±23% in Sm and Yb to ±33% in Nd, Gd and Dy. These are considerably larger than the uncertainty ±3.5% in the Ar^+ cross section obtained by Straub *et al.*[7] in the target gas-electron beam method and those ±(6–12)% in the various cross sections obtained by Wetzel *et al.*[8] and Freund *et al.*[9] in the fast neutral-beam method. The present total uncertainties are dominated by those in the ion current I_i, the intensity ratio I_C/I_S, and the average velocity $\langle v \rangle_{av}$. These are therefore key factors in obtaining the cross sections with better accuracy. For example, determination of $\langle v \rangle_{av}$ using the Doppler shift of resonance fluorescence excited by laser light would provide better accuracy for certain atomic species.

In the measurement of σ_T, much attention had to be paid to the determination of the ratio I_C/I_S. The ratio was observed to depend on the oven temperature (and hence on the metal sample used) and on the inner diameter of crucible used. Furthermore, the ratio seemed

Table II. Lowest binding energies of the subshell electrons and the appearance potentials of each lanthanide atom. Data for Eu atom are also included.

The binding energy (eV)[a]									
	Ba	Ce	Nd	Sm	Eu	Gd	Dy	Er	Yb
$6s$	5.2	6.2	5.6	5.7	5.8	6.5	5.9	6.1	6.3
$5d$	—	6.2	—	—	—	10.3	—	—	—
$4f$	—	8.7	7.9	9.2	10.3	17.4	7.6	7.1	?
$5p$	22.7	25.5	25.5	25.3	26.7	29.2	28.1	30.5	31
$5s$	37.9	42.2	43.3	45.2	46.5	46	51.6	55	58
$4d$	98	116.8	123.1	130.9	137.6	151.3	155.1	172	190
The appearance potential (eV)[b]									
	Ba	Ce	Nd	Sm	Eu	Gd	Dy	Er	Yb
1+	5.2	6.2	5.6	5.7	5.8	6.5	5.9	6.1	6.3
2+	15.2	16.4	16.3	16.7	16.9	18.2	17.6	18.0	18.4
3+	51.1	36.6	38.4	40.1	41.8	38.9	40.4	40.9	43.5
4+	98.2	73.4	78.8	81.5	84.4	82.9	81.9	83.4	87.2

a) Values on Ba, Ce, Sm, Eu and Gd refer to photoelectron studies of Richter *et al.*,[13,14] values on Nd and Dy to that of Kutluk,[16] values on Er to that of Ishijima,[15] and values on Yb to Solid-phase data.

b) Values calculated from the ionization energies in Table I-1 in the text book of Cowan.[12]

Table III. Numerical values of the total (apparent) cross sections σ_T. (in units of 10^{-16} cm^2) and total uncertanties.

	σ_T (200 eV)	σ_T (400 eV)	σ_T (600 eV)	σ_T (900 eV)	Total uncertainty (in %)
Ce	6.01	4.21	3.42	2.77	30
Nd	6.06	3.74	2.93	2.21	33
Sm	7.50	4.29	2.84	2.50	23
Eu	6.05	3.90	2.65	2.28	23
Gd	7.98	5.63	4.34	2.91	33
Dy	6.17	4.51	3.37	2.68	33
Er	4.28	3.05	2.39	1.81	29
Yb	5.48	3.69	2.84	2.28	23

to depend to a certain extent on the amount of metallic sample in the crucible. These phenomena indicate that the "virtual" source point, the point from which the inverse square law of the beam intensity is applicable, varies depending on these oven parameters. The measurement of the ratio was more difficult for elements which need higher temperature for vaporization, leading to larger uncertainties.

4.2 Ionization processes

4.2.1 General features of the partial cross sections

Before discussing the ionization processes, we summarize general features observed in the present partial cross sections.

(a) The σ_+ curves do not vary smoothly and have more or less structure, in contrast with those in inert-gas atoms. The structure varies delicately from atom to atom, and suggests the existence of certain indirect processes.

(b) The σ_{2+} curves, except that for Gd, increases quadratically near the threshold and appear to have structure in the higher energy region. The Gd^{2+} curve differs noticeably from others in the near-threshold behavior.

(c) Formation of triply-charged ions, the threshold of which ranges from 36.6 eV in Ce to 43.5 eV in Yb, is very weak until the electron energy passes over the ionization threshold of $5s$ electron, 42.2 eV in Ce to 58.0 eV in Yb.

(d) The Ce^{3+} and Nd^{3+} curves are such that a relatively sharper peak starting around the $4d$ ionization threshold is superimposed on a smooth curve due to the direct ionization of $5s$ electron. However, the $4d$ peak weakens with increase in Z and almost disappears in Eu and subsequent heavier lanthanides.

(e) The formation of quadruply-charged ions amounts to a considerable level at the $4d$ ionization thresholds, the first inner-shell threshold above the appearance potential of quadruply-charged ion.

These features will be key points in the discussion of ionization mechanism in the following subsections.

It would be necessary to consider the electronic states of target atoms. The Table of Martin[10] includes the information necessary for this purpose, that is, energy terms and energy levels of the several lowest configurations. Table V lists, as typical examples, parts of those lowest levels of Ce and Dy atoms and their relative populations calculated from briefly estimated operating temperatures of the oven. From this Table, we find that

Table IV. Numerical values of the counting cross sections σ_C. (in units of 10^{-16} cm^2)

Electron energy (eV)	Ce	Nd	Sm	Eu	Gd	Dy	Er	Yb
5.5	0.0	0.0	0.0	0.0	0.0	0.0	0.0	0.0
6.0	0.0	0.22	0.33	1.13	0.0	0.07	0.0	0.0
6.5	0.04	0.46	1.07	2.14	0.0	0.21	0.23	0.21
7.0	0.14	0.70	1.88	3.23	1.13	0.48	1.13	0.62
7.5	0.26	0.94	2.99	4.21	2.27	0.80	2.23	1.15
8.0	0.39	1.25	4.24	5.47	3.78	1.14	3.23	1.85
8.5	0.58	1.72	5.67	7.49	5.04	1.56	3.98	2.48
9.0	0.81	2.26	5.53	9.01	5.67	1.80	4.72	3.39
9.5	0.99	2.92	4.66	8.15	5.61	2.15	5.29	4.50
10.0	1.15	3.29	4.91	7.37	5.52	2.42	4.83	5.27
11	1.72	4.11	4.89	6.56	5.88	2.98	3.57	4.93
12	1.98	4.96	5.66	6.46	6.18	3.55	3.22	4.78
13	2.43	4.55	5.89	7.23	5.49	3.97	3.47	5.55
14	2.65	5.10	6.72	7.15	5.20	4.33	3.84	6.09
15	3.01	6.22	6.97	7.12	6.24	5.24	4.11	6.75
16	3.66	6.73	7.12	7.34	7.36	6.04	4.43	6.82
18	4.53	7.84	7.47	7.16	7.88	6.60	4.85	7.45
20	5.29	8.04	7.54	7.38	8.80	7.10	4.98	7.87
23	6.62	8.02	7.85	7.79	9.23	8.49	5.14	7.98
26	7.41	8.84	8.06	7.85	10.70	9.20	5.37	8.06
30	8.03	9.64	8.25	7.79	11.11	9.46	5.74	8.59
35	7.90	9.64	7.54	7.22	12.27	8.94	5.86	8.83
40	7.95	9.57	7.27	6.88	11.62	8.60	5.67	8.69
45	7.85	9.52	7.10	6.65	11.32	8.32	5.46	8.22
50	7.55	9.25	6.79	6.54	10.95	7.98	5.29	7.86
60	6.85	8.52	6.24	6.08	9.82	7.60	5.00	7.09
80	5.71	7.73	5.66	5.61	8.17	6.86	4.43	6.05
100	5.09	7.11	5.25	5.17	7.06	6.16	4.03	5.58
130	4.78	5.53	5.00	4.76	6.52	5.41	3.64	4.81
170	4.53	4.46	4.67	4.23	5.91	4.70	3.22	4.15
200	4.38	4.02	4.36	3.88	5.62	4.34	3.02	3.75
250	4.08	3.40	3.86	3.44	5.20	3.88	2.71	3.29
300	3.73	2.98	3.42	3.08	4.90	3.56	2.44	2.97
350	3.42	2.70	3.15	2.84	4.41	3.26	2.24	2.73
400	3.14	2.48	2.88	2.64	3.99	3.05	2.09	2.52
500	2.79	2.14	2.42	2.30	3.53	2.64	1.82	2.24
600	2.50	1.90	2.16	2.04	3.17	2.37	1.63	2.01
700	2.30	1.74	1.99	1.84	2.79	2.13	1.49	1.85
900	2.04	1.47	1.67	1.55	2.39	1.80	1.27	1.58

the situation depends largely on the element considered. For example, the ground state of Dy atom is $[\mathrm{Xe}]4f^{10}6s^2(^5I)$. The lowest level of the first excited $4f^{10}(^5I_8)5d6s(^3D)$ configuration lies at about 2.2 eV above the ground state. At evaporation temperature of about 1400 K, the population of this excited level is calculated to be only 1.2×10^{-8}, extremely small compared to unity, the population of ground configuration atoms. The same applies to Er and Yb atoms. On the other hand, the population calculations for the other lanthanides show that excited species are more or less included in the atomic beam from the oven. An extreme example of it is seen in Ce atom. We see that the target Ce beam includes various excited sublevels which belong to the ground configuration but different terms. In addition, the relative population of $^5H^{\mathrm{o}}$ term of $4f$ $(^2F^{\mathrm{o}})5d^2(^3F)6s$ $^4F_{\mathrm{J}}$ excited configuration amounts to 0.29. Thus, the present cross-section results on Ce, Nd, Sm and Gd are those obtained from such "mixed" target beams.

In the analysis of the experimental results, we assume, as a basis of consideration, that the cross section for direct ionization of an electron of individual subshell varies in the standard way: it increases almost linearly from its ionization threshold, reaches a maximum at about three to four times the threshold value, and then decreases slowly more than the initial rise. This assumption is based on a number of previous experimental and theoretical studies on various atomic species, and is considered to be reasonable. This assumption then allows us to identify several interesting indirect processes. We cannot discuss about the threshold behavior in detail because the energy spread of the impacting electron is wide (about 1.2 eV).

Table V. The lowest energy configurations and terms of neutral Ce and Dy atoms, and the relative population of sublevels calculated at individual evaporation temperature. The configurations and the terms refers to the Table of Martin.[10)]

Ce Configuration	Term	J	Level (eV)	Relatove population
$4f5d6s^2$	$^1G^o$	4	0.0	1.0
$4f5d6s^2$	$^3F^o$	2	0.02837	0.82
		3	0.20620	0.24
		4	0.38437	0.07
$4f5d6s^2$	$^3H^o$	4	0.15863	0.34
		5	0.27384	0.15
		6	0.49297	0.03
$4f5d6s^2$	$^3G^o$	3	0.17221	0.31
		5	0.52066	0.03
$4f(^2F^o)5d^2(^3F)6s(^4F)$	$^5H^o$	3	0.29373	0.13
		4	0.30223	0.13
		6	0.58851	0.02
		7	0.71937	0.01
Dy Configuration	**Term**	**J**	**Level (eV)**	**Relative population**
$4f^{10}6s^2$	^5I	8	0.0	1.0
		7	0.51258	0.01
		6	0.87416	0
		5	1.14209	0
		4	1.35456	0
$4f^{10}(^5I_8)5d6s(^3D)$	$^3[8]$	9	2.17152	0
		8	2.34370	0
		7	2.61287	0

4.2.2 Single ionization processes

It is probably reasonable to consider that the formation of singly charged ions is dominated by ionization of the $6s$ electron. The ionization of a $4f$ electron also leads, in most case, to formation of singly-charged ion, but its contribution is expected to be minor because of collapse of the $4f$ wavefunction. However, some of the single ionization curves show significant structure in the $4f$ ionization region, suggesting existence of certain indirect processes due to the $4f$ electron. The structure depends largely on the target atom: the structure in the Nd^+, Sm^+, Gd^+ and Yb^+ curves appears to be composed of several fine peaks of resonance feature, and the peak at 9.5 eV in the Er^+ curve is most prominent.

According to the Hartree–Fock calculation of levels of $4f^w$ configuration by Cowan,[11,12)] the energy range covered by those levels amounts to 12 eV for $4 \leq w \leq 10$ due to the strong Coulomb repulsion among the $4f$ electrons. The distribution of energy levels in such a wide energy range has been demonstrated in photoelectron spectroscopies.[13–16)]

We consider the partial curve of Sm^+ formation, as a typical example, for which related information is available in published papers. According to the photoelectron spectrum on Sm atom reported by Richter *et al.*,[13)] the ground $4f^66s(^{6,8}F)$ state of Sm^+ ion, formed by ionization of a $6s$ electron, lies at 5.7 eV above the ground $4f^66s^2(^7F)$ state of Sm atom. As is shown in Fig. 2 schematically, the $4f$-ionization states $Sm^+(4f^56s^2,^6H,^6F)$, $Sm^+(4f^56s^2,^6P)$, $Sm^+(4f^56s7s,^6H,^6F)$ and $Sm^+(4f^56s7s,^6P)$ lie at 9.2 eV, 11.9 eV, 16.3 eV and 19.0 eV, respectively, above the ground state of Sm atom. The former two states correspond to strongest photolines, and the former three are lower than the appearance potential of Sm^{2+} ion, 16.7 eV. It follows then that there are a number of excited neutral $4f$-hole states converging to these excited Sm^+ states, and most of these states can autoionize to Sm^+ ion with large probabilities.

The peak structure in the 9–18 eV region of the Sm^+ curve is possibly attributed to the excitation-autoionization process

$$Sm(4f^66s^2,^7F) + e^- \rightarrow Sm^*(4f^56s^2nl) + e^- \rightarrow Sm^+(4f^66s,^{6,8}F) + 2e^-.$$

Because some of the peaks are very sharp, Sm^+ ion may be produced *via* a temporary negative-ion resonance,

$$Sm(4f^66s^2,^7F) + e^- \rightarrow Sm^-(4f^56s^2n_1l_1n_2l_2) \rightarrow Sm^+(4f^66s,^{6,8}F) + 2e^-.$$

Such a negative-ion resonance has been observed in electron-impact ionization of alkaline atoms. For example, the excitation of a K atom to a metastable state has been proved to occur *via* the formation of core-excited negative ion resonance. The excited K atom thus produced can autoionize with a large probability, leading to formation of K^+ ion.[17,18)] A similar near threshold behavior has been observed in lithium,[19)] sodium,[20)] and caesium.[21)]

In the same way, the features seen on the lower energy

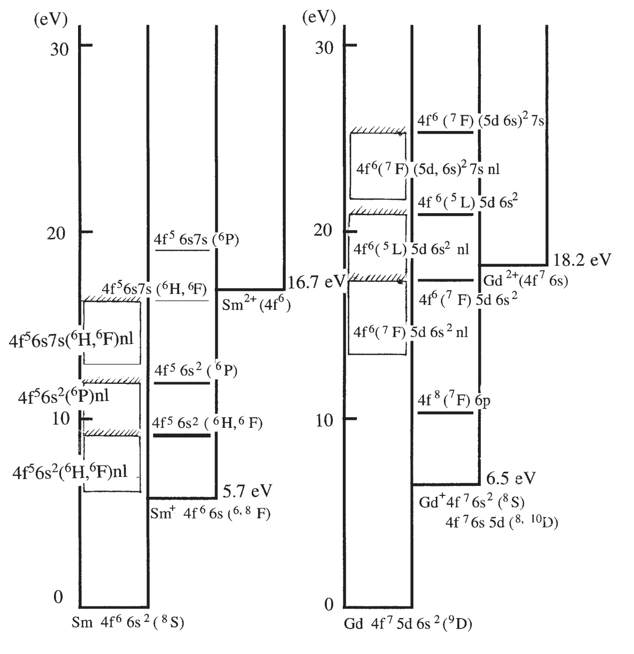

Fig. 2. Energy positions of the ground states of singly and doubly charged Sm and Gd ions and those of $4f$-ionized states of their singly-charged ions with respect to the ground states of individual neutral atoms. Squares in the column of each neutral state indicate the positions of loughly expected $4f$-hole excited states.

side of the maximum of other σ_+ curves are possibly attributed to formation of a $4f$-excited state $4f^{w-1}6s^2(5d)nl$ either *via* the direct excitation or *via* a temporary negative-ion state $4f^{w-1}6s^2(5d)n_1l_1n_2l_2$, w being the number of $4f$ electrons in the ground-state neutral atom. It is impossible at present to specify a definite excited state for each feature in the σ_+ curve because of lack of detailed information about $4f$-hole excited neutral levels.

4.2.3 Double ionization processes

The threshold of double ionization of Sm atom, 16.7 eV is fairly below the ionization thresholds of $5p$ electron, 25.3 eV. Consequently, only possible process below the $5p$ threshold is the direct double ionization process in which two outer shell electrons are ionized simultaneously. In this case, the threshold law[6] expects nearly quadratic increases as a function of the excess energy. The increase of the present Sm^{2+} curve near the threshold is approximately quadratic, in good agreement with this expectation. Above the $5p$ threshold, the main role in the Sm^{2+} formation is replaced by the Auger process following formation of $5p$-hole ionic states. According to the photoion-yield study of Dzionk *et al.*,[22] about 90% of Sm^+ ions in the $5p$-hole states decay to Sm^{2+} by Auger process at about 5 eV above the $5p$ ionization threshold. The same applies in the cases of other lanthanide elements studied with the exception of Gd case.

Very interesting is the Gd^{2+} curve whose growth near threshold is not quadratic but rather linear. One prominent difference between Gd and other lanthanides studied lies in the energy position of $4f$-ionization states relative to the ground state of doubly-charged ion.[13] Figure 2 shows such a difference through comparison with the Sm case, a typical case of the lanthanides. One finds that three $Gd^+(4f^{-1})$ states are identified and the higher two lie fairly above the ground Gd^{2+} state. This is in contrast to the other cases where main $4f$-hole states lie below the ground state of doubly charged ions. Thus one possibility in Gd is that certain neutral $4f$-hole levels, $4f^6(^5L)5d6s^2nl$, lying just above the double ionization threshold are excited, and decay to Gd^{2+} ion with emission of two electrons. The ionization of $4f$ electron leading to the two higher $4f$-ionization states may contribute to Gd^{2+} formation additionally.

The double ionization cross-section curves of Ce, Nd, Sm, Er, Dy and Yb atoms seem to have, more or less, structure in the higher-energy region. However, it is hard at present to find any correspondence between these structures and atomic energy levels.

4.2.4 Triple ionization processes

The cross-section curves for formation of triply-charged ions vary in relatively simple manner with increasing the impacting-electron energy, but depends significantly on the atomic number Z.

We note first the variation of the Ce^{3+} curve. Formation of Ce^{3+} ions, the threshold of which is 36.6 eV, is very weak until the electron energy passes over the ionization threshold of $5s$ electron (42.2 eV). Although the simultaneous ionization of three outer subshell ($5p$, $4f$, and $6s$) electrons is energetically possible, its probability is apparently quite small. An appreciable formation of Ce^{3+} ions starts at the $5s$ threshold, evidently indicating that Ce^{3+} ions here come mainly from Auger process following the ionization of $5s$ electron. The same explanation is applicable to other lanthanide atoms.

The Ce^{3+} curve, as in the case of Ba^{3+} curve,[1] has an additional onset starting around the $4d$ ionization threshold. This indicates evidently the opening of a new ionization channel due to the $4d$ electron. Physically very interesting are the shape and atomic number (Z) dependence of the $4d$ ionization curves. We see that the $4d$ cross section functions are prominently sharper than usual. Also we see that the $4d$ curve decreases in its magnitude with increasing Z and is out of sight in Eu and subsequent elements.

The sharper peak beyond the $4d$ threshold is presumably due to a kind of resonance process associated with the $4d$ electron from following two reasons. First, the $4d$ curve reaches its maximum at about 1.5 times the threshold value, apparently different from the direct ionization cases. Second, the shape of the $4d$ peak is similar to the resonance behavior above the $4d$ threshold observed in electron impact ionization of several heavier ions. Such a resonance behavior has been observed first in double ionization of Cs^+ ions by Hertling *et al.*[23] and later in double ionization of I^+ and Xe^{q+} ($q = 1$–4) ions by Achenback *et al.*,[24] in double ionization of Ba^+ ion by Hirayama *et al.*[25] and by Peart *et al.*[26] and in single ionization of Xe^{q+} ($q = 2$–6) by Griffin *et al.*[27] The resonance behavior in Cs^+ ion has been explained as *shape resonance* (i.e. potential barrier effect) by Younger[28] based on distorted-wave calculations. We note that similar structure was previously observed in the triple ionization of neutral Ba atom by Okudaira,[29] Ziesel and Abouaf,[30] and Dettmann and Karstensen.[31] though it is not explained as resonance in their papers.

One possible explanation of the Z dependent behavior of the $4d$ peak is gradual change in the resonance feature from the shape resonance (the open-channel resonance) to the autoionizing resonance (closed-channel resonance). A similar change in the resonance feature has been observed in the $4d$ photoabsorption of lanthanide atoms. This phenomenon is explained as the potential barrier effect: as the atomic number Z increases, the potential barrier for the f electron lowers from above to below the $4d$ ionization threshold, and the $4f$ wavefunction collapses inside the $5s$ and $5p$ wavefunctions correspondingly.[10,32] This collapse results in a strong $4d$–$4f$ interaction because of large overlapping of the two wavefunctions. The eventual result is that the shape resonance in the Ba and lighter lanthanides changes into the autoionizing resonance $4d^{10}4f^n \to 4d^94f^{n+1} \to 4d^{10}4f^{n-1}$ in the heavier lanthanides. If a similar explanation applies to the present case, the potential curve should be that for an incident f electron, and the parent of the resonance[33] should be neutral atom of the $4d^95s^25p^64f^n6s^2(5d)nl$ excited configuration. It would be expected that as Z increases, the resonance level in the heavior lanthanides lowers below the $4d$ ionization limit, and the possibility of forming triply-charged ions

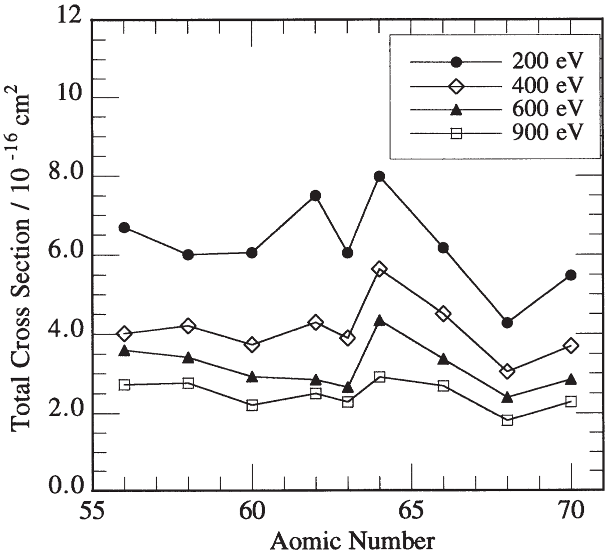

Fig. 3. The absolute total (apparent) cross sections at electron energies 200, 400, 600 and 900 eV as a function atomic number Z.

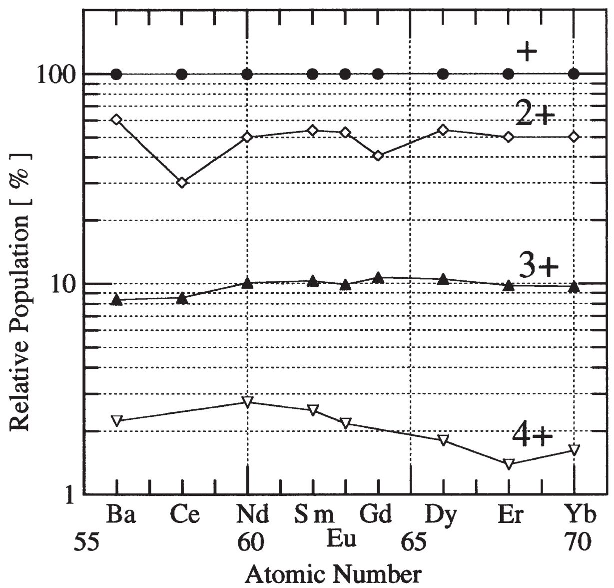

Fig. 4. Populations of doubly, triply and quadruply charged ions relative to that of singly-charged ions. The population of singly-charged ions is taken to be 100.

vanishes. The resonance behavior in the triple ionization curves will be reported in more detail in a separate paper in which additional experimental data on La, Pr and Ho atoms will be included.

4.2.5 Quadruple ionization of lanthanide atoms

Partial cross sections for quadruple ionization have been measured for Sm and Yb atoms as well as Eu atom reported in I.[1] The appearance potentials of Sm^{4+} and Yb^{4+} ions are 81.5 eV and 87.2 eV, respectively. These energies are considerably lower than the lowest ionization thresholds of 4d electron (Sm: 130.9 eV, Yb: 190 eV). We note that formation of Sm^{4+} and Yb^{4+} ions amounts already to a considerable level at the 4d thresholds. This trend is also seen in the Eu case.[1] In the Sm case, for example, the energy range from the appearance potential 81.5 eV to the 4d ionization threshold 130.9 eV is so wide, and hence it is not likely that the direct multiple ionization process plays an important role entirely in this range. The simultaneous ionization of four outer-shell electrons is in principle possible, but its probability should be extremely small. It follows then that certain indirect processes play non-negligible roles. Probable processes are shake-up and/or shake-off processes associated with 5s and 5p ionization followed by Auger process(es).

4.3 Comparisons among σ_T's and the charge-state distributions

Comparison among the absolute total cross sections σ_{T} and that among the charge state distributions obtained for the lanthanide and Ba atoms give us further interesting information. Figure 3 shows the σ_{T} values at electron energies 200, 400, 600 and 900 eV as a function of atomic number Z. Figure 4 shows the charge-state distribution at 400 eV also as a function of Z. The distribution is expressed as the population of the doubly-, triply- and quadruply-charged ions relative to that of the singly-charged ions.

One interesting feature is the behavior of the relative population of the doubly-charged ions. The relative populations of Ce^{2+} and Gd^{2+} ions are 30% and 40%, respectively, which are remarkably smaller than those (about 55%) for the other lanthanide atoms (we have obtained recently 38% as the relative population of La^{3+}). When the 4f subshell is occupied successively in the lanthanide series, exceptions occur at Ce and Gd atoms as well as at La atom. In these atoms, an additional electron occupies the 5d shell instead of the 4f shell. The ionization of 5d electron results in formation of a singly-charged ion. Also the ionization of 4f electron results mainly in formation of singly-charged ion. On the other hand, the expectation values of radius r for the 5d and 4f orbitals in these atoms are about three-quarters and a quarter, respectively, of that of 6s electron.[11] The smaller 4f radius is ascribed to the collapse of the 4f wavefunction. Consequently, the 5d electron is expected to provide a considerably larger cross section than the 4f electron does, making the population of single ionization relatively larger. This enhancement of the single ionization results in decrease in the apparent relative populations of multiple ionization, especially of double ionization.

We cannot mention many about the Z dependence of the absolute cross sections σ_{T}, because the estimated uncertainties are comparable with the magnitude of the variation of σ_{T} with Z. However, it is certain that Gd atom has relatively larger total cross sections. From the same reason just mentioned above, the drastic increase in σ_{T} value from Eu to Gd is explained presumably by the occupation of the 5d shell in Gd atom.

§5. Conclusions

We have investigated the electron impact ionization of lanthanide atoms through the measurement of the absolute total (apparent and counting) and the absolute charge-separated partial cross sections. The purpose was to establish experimental technique for metallic elements which require high temperatures for vaporization, to understand the ionization processes in these atoms, and to provide cross-section data to related fields. The measurements on atomic species Ce, Nd, Gd, Dy and Er are made for the first time.

From the physical point of view, the present results can be summarized as follows.

(i) Some of the single ionization cross-section curves show complicated structure in the region the $4f$ ionization thresholds, possibly attributed to the formation of autoionizing $4f$-excited states *via* the direct process or *via* the temporal negative-ion resonance.

(ii) The double and triple ionizations are dominated by the direct ionization of $5p$ and $5s$ inner-shell electrons, respectively, followed by Auger process(es).

(iii) Evidences of shake-up and/or shake-off processes associated with $5p$ and $5s$ electron are observed in the quadruple ionization curves.

(iv) The $4d$ ionization appears as a peak of shape resonance feature in the Ce^{3+} and Nd^{3+} curves. The $4d$ peak, however, decreases in magnitude with increasing the atomic number Z and disappears beyond Eu atom. This is possibly attributed to the change in the resonance feature from the shape resonance to the autoionization resonance due to the lowering of the barrier of the double-well potential for f electron in the higher Z atoms.

Acknowledgements

We would like to express Dr. Takemasa Shibata of Japan Atomic Energy Research Institute for valuable discussion and comments. This work was partially supported by the Grant-in-Aid for Scientific Researches (07640537) from the Ministry of Education, Culture, Sports, Science and Technology.

1) S. Yagi and T. Nagata: J. Phys. Soc. Jpn. **69** (2000) 1374.
2) T. J. Jones: Phys. Rev. **29** (1927) 822.
3) L. L. Shimon, P. N. Volovich and M. M. Chiriban: Zh. Tekh. Fiz. **59** (1989) 64.
4) T. D. Mark: Int. J. Mass Spectrom. Ion Phys. **45** (1982) 125.
5) K. J. Ross and B. Sonntag: Rev. Sci. Instrum. **66** (1995) 4409.
6) L. J. Kieffer and G. H. Dunn: Rev. Mod. Phys. **38** (1966) 1.
7) H. C. Straub, P. Renult, B. G. Lindsay, K. A. Smith and R. F. Stebbings: Phys. Rev. A **52** (1995) 1115.
8) R. C. Wetzel, F. A. Baiocchi, T. R. Hayes and R. S. Freund: Phys. Rev. A **35** (1987) 559.
9) R. S. Freund, R. C. Wetzel, R. J. Shul and T. R. Hayes: Phys. Rev. A **41** (1990) 3575.
10) W. C. Martin, R. Zalubas and L. Hagan: *Atomic Energy Levels—The Rare-Earth Elements* (U.S. GPO, Washington, D.C., 1978) Natl. Bur. Stand. Ref. Data Ser., Natl. Bur. Stand. (U.S.) Circ. No. 60.
11) R. D. Cowan: *The Theory of Atomic Structure and Spectra* (University of California Press, Berkeley, 1981) p. 598.
12) R. D. Cowan: Nucl. Instrum. Methods **110** (1973) 173.
13) M. Richter, M. Meyer, M. Pahler, E. Prescher, E. v. Raven, B. Sonntag and H. E. Wetzel: Phys. Rev. A **40** (1989) 7007.
14) M. Richter, M. Meyer, M. Pahler, E. Prescher, E. v. Raven, B. Sonntag and H. E. Wetzel: Phys. Rev. A **39** (1989) 5666.
15) H. Ishijima: Thesis, Meisei University, 1995.
16) G. Kutluk: Doctoral Thesis, Meisei University, 1993.
17) A. A. Borovik, H. L. Rojas, G. C. King and E. Yu Remeta: J. Phys. B **32** (1999) 4225.
18) B. Feuerstein, A. N. Grum-Grzhimailo and W. Mehlhorn: J. Phys. B **32** (1999) 4547.
19) A. A. Borovik and V. N. Krasilinec: J. Phys. B **32** (1999) 1941.
20) B. Feuerstein, A. N. Grum-Grzhimailo and W. Mehlhorn: J. Phys. B **31** (1998) 593.
21) V. Pejčev and K. J. Ross: J. Phys. B **10** (1977) L291.
22) C. Dzionk, W. Fielder, M. von Luck and P. Zimmermann: Phys. Rev. A **39** (1989) 1780.
23) D. R. Hertling, R. K. Feeney, D. W. Hughes and W. E. Sayle II: J. Appl. Phys. **8** (1982) 5427.
24) Ch. Achenback, A. Muller and E. Salzborn: Phys. Rev. Lett. **50** (1983) 2070.
25) T. Hirayama, S. Kobayashi, A. Matsumoto, S. Ohtani, T. Takayanagi, K. Wakiya and H. Suzuki: J. Phys. Soc. Jpn. **56** (1987) 851.
26) B. Peart, S. J. T. Green and J. W. G. Thomson: J. Phys. B **26** (1993) 149.
27) D. C. Griffin, C. Bottcher, M. S. Pindzola, S. M. Younger, D. C. Gregory and D. H. Grandall: Phys. Rev. A **29** (1984) 1729.
28) S. M. Younger: Phys. Rev. Lett. **56** (1986) 2618.
29) S. Okudaira: J. Phys. Soc. Jpn. **29** (1970) 409.
30) J. P. Ziesel and R. Abouaf: J. Chim. Phys. **64** (1967) 702.
31) J.-M. Dettmann and F. Karstensen: J. Phys. B **15** (1982) 287.
32) A. R. P. Rau and U. Fano: Phys. Rev. **167** (1968) 7.
33) G. J. Schulz: Rev. Mod. Phys. **45** (1973) 378.